Available online at www.sciencedirect.com
SCIENCE DIRECT®
International Journal of Plasticity 22 (2006) 557–580
INTERNATIONAL JOURNAL OF Plasticity
www.elsevier.com/locate/ijplas

# A plane stress yield function for anisotropic sheet material by interpolation of biaxial stress states

H. Vegter [a,*], A.H. van den Boogaard [b]

[a] *Corus Research Development and Technology, P.O. Box 10000, 1970 CA IJmuiden, The Netherlands*
[b] *Faculty of Engineering Technology, University of Twente, P.O. Box 217, 7500 AE Enschede, The Netherlands*

Received 12 December 2003
Available online 28 July 2005

**Abstract**

An anisotropic plane stress yield function based on interpolation by second order Bézier curves is proposed. The parameters for the model are readily derived by four mechanical tests: a uniaxial, an equi-biaxial and a plane strain tensile test and a shear test. In case of planar anisotropy, this set of tests must be repeated for a number of directions. An arbitrary number of directions can be incorporated in the model. This flexibility can be used to describe, e.g., the yield stress and *R*-value as a function of the loading direction more accurately than with other common analytical yield functions. The relevance of an accurate description of the yield locus and the flexibility of the proposed yield function are demonstrated by the prediction of forming limit diagrams. It is demonstrated that the sensitivity of the FLD to small changes in the yield locus can also be used to determine some of the material parameters by inverse analysis.


*Keywords:* Constitutive modelling; Yield function; Anisotropic materials; Bézier curve; Forming limits

* Tel.: +31 251 499634; fax: +31 251 470432.
*E-mail address:* henk.vegter@corusgroup.com (H. Vegter).

0749-6419/$ - see front matter 
doi:10.1016/j.ijplas.2005.04.009

## 1. Introduction

The application of simulation models in sheet metal forming in the automotive industry has proven to be beneficial to reduce tool costs in the design stage and for optimising current processes. Moreover, with a view to environmental, economic and safety concerns, the car manufacturers need to design lighter and safer vehicles in ever shorter development times. This means that the components have to be designed more critically regarding their forming behaviour. This in turn means that the material models used in forming simulations need to have a high accuracy. In this paper, the focus is on the yield function description, but it is noted that an accurate description of the hardening is equally important for successful simulations.

Rolled sheet usually exhibits an orthotropic symmetry, in which the rolling direction, transverse direction and normal direction are lines of symmetry. Many yield functions have been defined in order to represent the elastic limit and subsequent plastic deformation for different sheet materials. The quadratic Hill '48 model (Hill, 1948) was successfully applied for steel sheet over a long period and is still widely used. The parameters, used in the plane stress version of the Hill '48 model are usually determined by uniaxial tensile tests at 0°, 45° and 90° with respect to the rolling direction. The common faith in the model led to the notion of 'anomalous behaviour' of aluminium (Woodthorpe and Pearce, 1970), for which the equi-biaxial yield stress was higher than the uniaxial yield stress while the $R$-value was less than 1. This is in contradiction with the Hill '48 model and it clearly showed that the anisotropic behaviour of metals in general, should not be based on uniaxial tests only.

Subsequent models by Hill (1979, 1990, 1993) improved the description of the yield locus, e.g., for aluminium by also considering the equi-biaxial yield stress as a parameter. Barlat and co-workers developed another series of yield functions, mainly focused on the description of the plastic deformation of aluminium. The first two models, Yld89 and Yld91 (Barlat and Lian, 1989; Barlat et al., 1991) focus on sheet and bulk forming, respectively. Model parameters for Yld89 are determined based on uniaxial tensile tests only, considering either the yield stress or the $R$-value in the 0°, 45° and 90° directions. For the plane stress version of Yld91 the equi-biaxial yield stress is considered additionally. Karafillis and Boyce (1993) introduced an 'isotropy plasticity equivalent' (IPE) in order to define anisotropic behaviour with isotropic functions. This was used by Barlat et al. (1997a,b, 2003) in the subsequent models Yld94, Yld96 and Yld2000. These models are typically used for sheet material and the parameters are determined from the uniaxial yield stress and the $R$-value and the equi-biaxial yield stress. Depending on the model, the 0° and 90° directions are used or the 0°, 45° and 90° directions. For Yld2000, also the strain ratio in equi-biaxial stress is used. An extension of the Barlat and Lian (Yld89) model was recently given by Banabic et al. (2003). This model has 6 material parameters that are fitted to the uniaxial yield stress and $R$-value in 0°, 45° and 90° directions and the equi-biaxial yield stress. Later on Banabic et al. (2005) presented their model BBC2002 and an improved version BBC2003. These models can be expressed as direct derivatives of Yld2000. A combination of the Karafillis and Boyce model with Yld91 led Bron and Besson (2004) to a 14-parameter 3D yield function. The

parameters were fitted to the uniaxial yield stress and $R$-value in the 0°, 45° and 90° directions and non-uniform tests with notched specimens. Recently, Barlat et al. (2005) presented two 3D yield functions (Yld2004-18p and Yld2004-13p) with 18 and 13 parameters, respectively. In a sheet forming application, out-of-plane yield stresses were determined by polycrystal analysis. Wu et al. (2003) and Butuc et al. (2002) presented an evaluation of some of the above yield functions and their influence on the prediction of a forming limit curve.

All yield functions referred above are global functions of the 6 (general) or 3 (plane stress) stress components. The complex geometry of the yield locus for some materials requires the definition of complicated non-quadratic yield functions. In this paper another approach is proposed, initially developed for planar isotropic sheet material (Vegter et al., 1995) and later extended for planar anisotropic material (Pijlman et al., 1998; Vegter et al., 1999b; Pijlman, 2001). The yield locus in the plane stress and principal stress space $(\sigma_1, \sigma_2)$ is explicitly described by a set of quadratic Bézier interpolations between pre-determined stress states. By allowing the Bézier parameters to depend on the angle between the first principal stress and the rolling direction, a highly adaptable planar anisotropic yield criterion is created. Very recently Tong et al. (2004) also used this approach for the description of a yield locus which includes the rotation of the material axis frame regarding plastic spin.

Apart from uniaxial and equi-biaxial test data, the current model also applies plane strain and pure shear data. The interpolation with Bézier curves is described in Section 2. Based on the description of the yield locus, a yield function is developed in Section 3 that can be used in standard return mapping algorithms. In Section 4, the flexibility of the yield function is demonstrated by an accurate prediction of the forming limit diagram for a BCC material, as well as for an FCC material.

## 2. Yield locus description

### 2.1. Bézier curves

The first step in the definition of the new yield function is the description of a plane stress yield locus in the principal stress space. In this two-dimensional principal stress space, a stress point is represented by the vector $\vec{\sigma} = \{\sigma_1, \sigma_2\}^{\mathrm{T}}$. Every plane stress situation can now be represented by the principal stresses $\vec{\sigma}$ and the angle $\theta$ between the 1st principal axis and the rolling direction. For a polycrystalline metallic material the yield locus will be smooth, i.e., it will not contain corners and the yield function will be continuously differentiable. Instead of selecting a global function that will result in a more or less appropriate yield locus, we can construct a yield locus piece by piece, as long as the smoothness is maintained. A suitable mathematical description to achieve this is given by a second order Bézier curve (Bézier, 1986) as presented in Fig. 1.

The second order Bézier function is based on two reference stress points $\vec{\sigma}_i$ and $\vec{\sigma}_j$, and a hinge point $\vec{\sigma}_h$. Between both reference points, the yield locus is then locally defined by

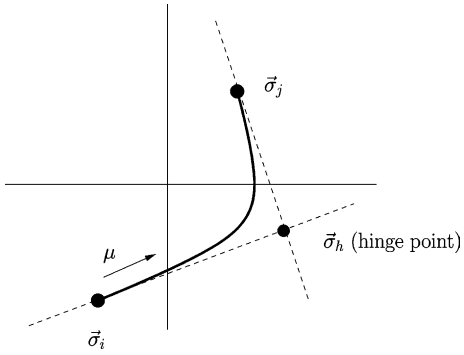


Fig. 1. Second order Bézier curve between two reference stress points.

$$\vec{\sigma}_{\text{locus}} = \vec{\sigma}_i + 2\mu(\vec{\sigma}_h - \vec{\sigma}_i) + \mu^2\left(\vec{\sigma}_i + \vec{\sigma}_j - 2\vec{\sigma}_h\right), \quad 0 \leqslant \mu \leqslant 1. \tag{1}$$

Differentiation with respect to $\mu$ readily shows that the resulting curve is tangential to $\vec{\sigma}_h - \vec{\sigma}_i$ at $\vec{\sigma}_i$ and tangential to $\vec{\sigma}_j - \vec{\sigma}_h$ at $\vec{\sigma}_j$, respectively at $\mu = 0$ and $\mu = 1$.

Four characteristic stress states are selected as reference points: the equi-biaxial point, the plane strain point, the uniaxial point and the pure shear point (Fig. 2). Between the 4 stress points, 3 Bézier curves are used to interpolate the yield locus between the equi-biaxial and plane strain point, between the plane strain and the uniaxial point and between the uniaxial and pure shear point. These four characteristic points are chosen because they can be determined with relatively simple mechanical tests. At yielding, not only the stresses but also the strain rates in the principal stress directions are recorded. For an associated flow rule the strain rate direction is coaxial with the normal to the yield locus and therefore also defines the tangent to the yield locus. The hinge points can be determined as the intersection of the tangents at the two reference stress points as elaborated in Appendix A. By determining the position of the hinge points in this way, it is assured that the constructed yield locus

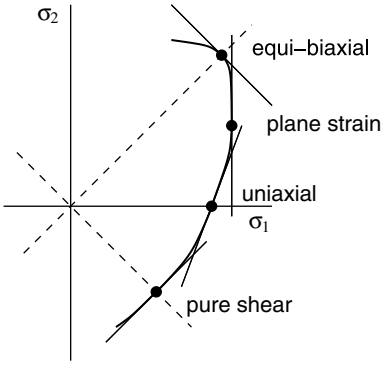


Fig. 2. Basic stress points and tangents to the Vegter yield locus.

is smooth, i.e., it does not contain corners and the normal to the yield locus is well defined at all positions.

As shown in Fig. 3, 12 reference points and normals are required to describe a complete yield locus for a particular direction of the principal stresses. It is assumed, however, that reversed loading leads – at least initially – to yielding at the same absolute stress values. This results in a point-symmetric yield locus with respect to the origin. For planar isotropic material $\sigma_1$ and $\sigma_2$ can be exchanged and the yield locus is symmetric with respect to the line $\sigma_1 = \sigma_2$. Therefore only 4 reference points and normals need to be specified for planar isotropic material. In Section 2.2, the model will be extended for planar anisotropic material behaviour.

Isotropic hardening can be incorporated in the interpolated criterion by multiplying the values for all reference points with a scalar. For this purpose, it is convenient to normalise the reference points with, e.g., the initial uniaxial yield stress in the rolling direction. The actual yield locus is then obtained after multiplication of all reference points with the current value of the flow stress $\sigma_f$. The normalised yield locus is denoted by the symbol $\vec{f}$. The yield locus is then written as $\vec{\sigma}_{\text{locus}} = \sigma_f \vec{f}$ with:

$$\vec{f} = \vec{A} + 2\mu\left(\vec{B} - \vec{A}\right) + \mu^2\left(\vec{A} + \vec{C} - 2\vec{B}\right), \quad 0 \leqslant \mu \leqslant 1, \tag{2}$$

where $\vec{A}$ and $\vec{C}$ are normalised reference points and $\vec{B}$ the corresponding hinge point. Depending on the position on the yield locus, $\vec{A}$ and $\vec{C}$ represent the normalised equi-biaxial, plane strain, uniaxial or pure shear stress points. The normalised reference points in the range where $\sigma_1 \geqslant \sigma_2$ and $\rho \geqslant -1$ are denoted by the equi-biaxial point $\vec{f}_{\text{bi}}$, the plane strain point $\vec{f}_{\text{ps}}$, the uniaxial point $\vec{f}_{\text{un}}$ and the shear point $\vec{f}_{\text{sh}}$. The components in the first principal stress direction of these points are simply referred to as the equi-biaxial factor, plane strain factor, uniaxial factor and shear factor $f_{\text{bi}}, f_{\text{ps}}, f_{\text{un}}$ and $f_{\text{sh}}$, respectively. The yield locus normals are denoted by the scalar

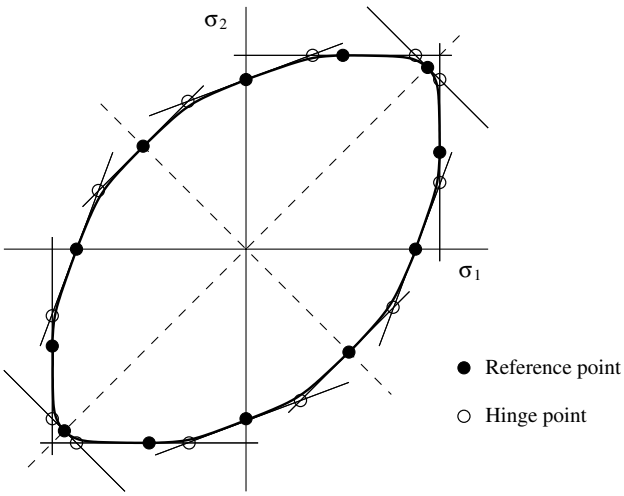


Fig. 3. A complete interpolated yield locus, and tangents in the reference points.

strain ratios $\rho_{bi}$, $\rho_{ps}$, $\rho_{un}$ and $\rho_{sh}$, respectively, where $\rho = \dot{\varepsilon}_{\sigma_2}/\dot{\varepsilon}_{\sigma_1}$. Here, we write $\dot{\varepsilon}_{\sigma_1}$ to denote the strain rate in the direction of the first principal stress. Note that for normal anisotropic materials this need not be the same direction as the first principal strain rate $\dot{\varepsilon}_1$.

Some relations and conditions for the stress factors and strain ratios are given in Table 1. Additionally, the parameters must be chosen, such that a convex yield locus evolves. In the principal stress plane simple linear relations can be obtained between stress points and strain ratios, in order to achieve convexity, by reference to Fig. 2. For planar isotropic material this condition is sufficient, but for anisotropic material it should be checked numerically whether the second derivative of the yield function to the stresses is positive definite for all stresses.

Kinematic hardening can be incorporated easily by subtracting the back stress from the total stress and using the resulting effective stress instead of $\boldsymbol{\sigma}$ in the yield locus. This was elaborated for the current model by Pijlman (2001), but will not be used in this paper for clarity.

### 2.2. Planar anisotropy

For planar anisotropic sheet material, the yield locus and hence the (normalised) reference points and their normals will depend on the angle between the first principal stress and the rolling direction. The angular dependency of the reference points and strain ratios can be presented as Fourier series in $\theta$. This function is not completely arbitrary.

Firstly, because the stresses are periodic with a period $\pi$, a rotation of the specimen with an angle $\pi$ does not change the stress situation and therefore the normalised yield locus $\vec{f}$ should be independent of a rotation by $\pi$:

$$\vec{f}(\theta) = \vec{f}(\theta + \pi). \tag{3}$$

This condition is fulfilled by using sine and cosine terms that depend on a multiple of $2\theta$.

In this paper we only consider orthotropic materials and therefore symmetry along the $\theta = 0$ and $\theta = \pi/2$ axis is required:

$$\begin{aligned} &\vec{f}(\theta) = \vec{f}(-\theta), \\ &\vec{f}\left(\frac{1}{2}\pi + \theta\right) = \vec{f}\left(\frac{1}{2}\pi - \theta\right). \end{aligned} \tag{4}$$

This is fulfilled if only the even ($\cos 2i\theta$) terms in the Fourier series are used and not the odd ($\sin 2i\theta$) terms. For a particular angle $\theta$ the interpolated normalised yield

Table 1
Relations and conditions for stress factors and strain ratios

| | Equi-biaxial | Plane strain | Uniaxial | Pure shear |
|---|---|---|---|---|
| Stress factor | $f_{bi_1} = f_{bi_2}$ | | $f_{un_2} = 0$ | Eq. (7) |
| Strain ratio | Eq. (9) | $\rho_{ps} = 0$ | $\rho_{un} = \frac{-R}{R+1}$ | $\rho_{sh} = -1$ |

locus only depends on the reference points and corresponding normals and therefore the directional dependency must be included in the reference points and corresponding strain ratios:

$$\begin{aligned} \vec{f}_k(\theta) &= \sum_{m=0}^{n} \vec{\varphi}_{km} \cos 2m\theta, \quad k \in \{\text{ps, un, sh}\}, \\ \rho_{\text{un}}(\theta) &= \sum_{m=0}^{n} \varrho_m \cos 2m\theta, \end{aligned} \tag{5}$$

where $\vec{\varphi}_{km}$ and $\varrho_m$ are Fourier parameters.

The pure shear point is defined as the point on the yield locus where $\rho = -1$. For planar anisotropic material, this is not necessarily the point were $\sigma_2 = -\sigma_1$. In pure shear, however, a stress reversal leads to an equivalent pure shear situation rotated by 90°, so the following condition holds:

$$f_{\text{sh}_2}(\theta) = -f_{\text{sh}_1}\left(\theta + \frac{1}{2}\pi\right) \tag{6}$$

or in combination with (4):

$$f_{\text{sh}_2}(\theta) = -f_{\text{sh}_1}\left(\frac{1}{2}\pi - \theta\right). \tag{7}$$

So, for an orthotropic material, only the first principal shear stress needs to be specified for angles $0 \leqslant \theta \leqslant 1/2\pi$.

Alternatively, the pure shear point can be defined as the point where $\sigma_2 = -\sigma_1$. In that case, $f_{\text{sh}}$ and $\rho_{\text{sh}}$ must be specified for angles $0 \leqslant \theta \leqslant 1/4\pi$. The former definition has the advantage that a prescribed strain reflects the shear test better than a prescribed stress. A prescribed strain is also advantageous in a polycrystal analysis.

The equi-biaxial stress point $\vec{f}_{\text{bi}}(\sigma_1 = \sigma_2)$ is independent of the orientation $\theta$ and the strain ratio in the equi-biaxial stress point can therefore be determined from a straightforward rotation of the strain rate tensor:

$$\begin{aligned} \dot{\varepsilon}_{\sigma_1}(\theta) &= \frac{1}{2}[\dot{\varepsilon}_1(0) + \dot{\varepsilon}_2(0)] + \frac{1}{2}[\dot{\varepsilon}_1(0) - \dot{\varepsilon}_2(0)]\cos 2\theta, \\ \dot{\varepsilon}_{\sigma_2}(\theta) &= \frac{1}{2}[\dot{\varepsilon}_1(0) + \dot{\varepsilon}_2(0)] - \frac{1}{2}[\dot{\varepsilon}_1(0) - \dot{\varepsilon}_2(0)]\cos 2\theta, \end{aligned} \tag{8}$$

where the strain rates $\dot{\varepsilon}_1(0)$ and $\dot{\varepsilon}_2(0)$ are the principal strain rates when the principal stresses are in the rolling and transverse direction.[1] The directional dependency of the equi-biaxial strain ratio is then

$$\rho_{\text{bi}}(\theta) = \frac{(\rho_{\text{bi}}(0) + 1) + (\rho_{\text{bi}}(0) - 1)\cos 2\theta}{(\rho_{\text{bi}}(0) + 1) - (\rho_{\text{bi}}(0) - 1)\cos 2\theta}, \tag{9}$$

so only $\rho_{\text{bi}}(0)$ has to be specified.

[1] For orthotropic materials the principal strain rate directions coincide with the principal stress directions for $\theta = 0$.

The 4 reference points indicated in Fig. 2 with $\sigma_1 \geqslant \sigma_2$ represent exactly the 4 reference points for $\sigma_1 \leqslant \sigma_2$ for a specimen rotated by 90°. Therefore only the stress factors and strain ratios for the region where $\sigma_1 \geqslant \sigma_2$ and $\rho \geqslant -1$ need to be specified as a function of $\theta$. The part of the yield locus where $\sigma_1 + \sigma_2 < 0$ is determined by the assumption that the initial yield stress in compression is equal to that in tension.

### 2.3. Determination of material parameters

The flexibility of the proposed yield function inevitably leads to a large number of material parameters. The equi-biaxial point and corresponding strain ratio need to be determined only in the principal material directions. If planar anisotropic behaviour has to be included, all other stress points and strain ratios should be determined for a number of directions. For orthotropic sheet the first three terms in the Fourier series are sufficient to describe the development of four ears in cylindrical cup deep drawing. This can be based on data at 0°, 45° and 90°.

For every direction, plane strain, uniaxial and shear data must be specified. The data can be obtained from experiments or from polycrystal analysis. In the latter case, it is straightforward to derive the stress points and strain ratios in any required direction and stress mode. By increasing the number of Fourier terms, the proposed yield function can approximate the yield surface obtained from polycrystal analysis accurately. An experimental determination of the material parameters is more laborious.

The uniaxial stress point and strain ratio can be obtained by standard tensile tests determining the yield stress and the $R$-value for specimens at different angles with respect to the rolling direction. The other reference points were chosen such that their experimental determination is, although less common than the tensile test, relatively easy.

The authors determine the reference points with unidirectional experiments only (Vegter, 1991; Vegter et al., 1999a, 2003; Pijlman, 2001). The equi-biaxial stress point and strain ratio are obtained from compression in the normal direction of a stack of sheet specimens, assuming that the hydrostatic stress has no effect on the plastic deformation (Tozawa, 1978; An and Vegter, 1998; Barlat et al., 2003).

The plane strain and pure shear point are determined with a test specimen as presented in Fig. 4. Only the small white area in the middle is the deformation zone. Vertical translation of the upper clamp in an ordinary tensile testing machine gives a plane strain deformation. In this way only the first principal stress can be measured and the minor principal stress is assumed to lie in the middle between the two neighbouring hinge points. Horizontal translation of the upper clamp gives a simple shear deformation, in which case an additional bearing must suppress rotation of the specimen. For the initial yield stress in pure shear, the simple shear test can be used rotated over 45°. Here also, the stress in the specimen $x$-direction can not be measured and the relation $\sigma_1 = -\sigma_2 = \sigma_{xy}$ is assumed.

Alternatively, the plane strain and equi-biaxial points can be obtained by biaxial loading of cruciform specimens as described, e.g., by Müller and Pöhlandt (1996); Hoferlin et al., 1998 and Kuwabara et al. (2000, 2002). With these types of

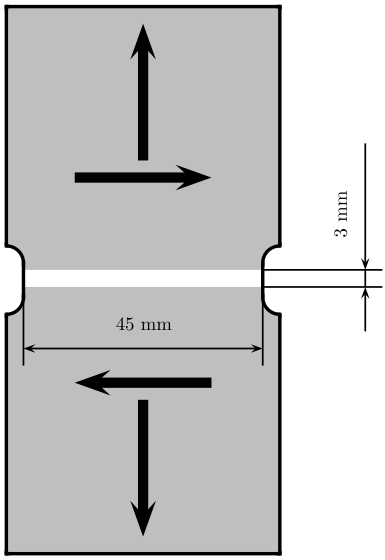


Fig. 4. Plane strain and simple shear specimen (gray part is clamped).

experiments the yield locus can be scanned between the uniaxial and the equi-biaxial points in tension. A disadvantage of these tests is that it requires a relatively complex biaxial loading frame and force control compared to unidirectional tests. The hydraulic bulge test can be an alternative to determine the equi-biaxial point, requiring accurate measurement of curvatures.

Notice that with an equal number of directions and Fourier terms, the Fourier coefficients are obtained by solving a linear set of equations for every stress and strain rate separately. There is no need to solve a set of nonlinear equations as with many other advanced material models. E.g., for 3 Fourier terms ($n = 2$ in Eq. (5)), experiments are usually performed in the 0°, 45° and 90° directions with respect to the rolling direction. The cosine coefficients for the strain ratios are then calculated from:

$$\begin{aligned} \varrho_0 &= \frac{\rho_{\mathrm{un}}(0^\circ) + 2\rho_{\mathrm{un}}(45^\circ) + \rho_{\mathrm{un}}(90^\circ)}{4}, \\ \varrho_1 &= \frac{\rho_{\mathrm{un}}(0^\circ) - \rho_{\mathrm{un}}(90^\circ)}{2}, \\ \varrho_2 &= \frac{\rho_{\mathrm{un}}(0^\circ) - 2\rho_{\mathrm{un}}(45^\circ) + \rho_{\mathrm{un}}(90^\circ)}{4}, \end{aligned} \tag{10}$$

and the coefficients for the stress points are calculated likewise.

If all or some of the reference points or strain ratios are known in more than 3 directions, the number of Fourier terms can easily be extended, so that the yield function matches these values exactly. As an example, in Figs. 5 and 6, the $R$-values and uniaxial stress factors of an AA 6016 sheet are presented, that were

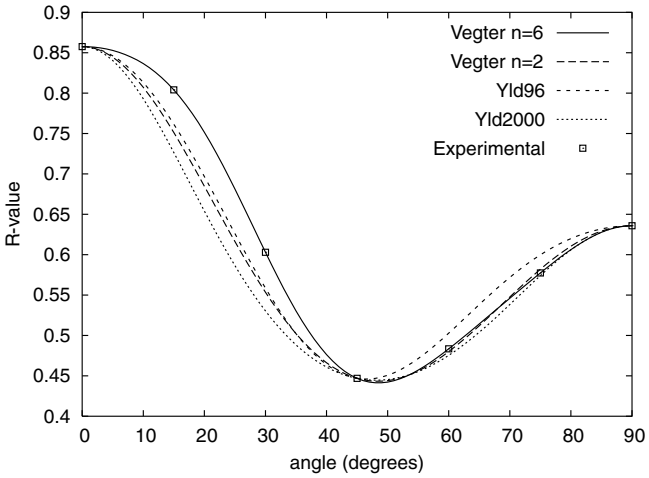


Fig. 5. Predicted and experimental $R$-values.

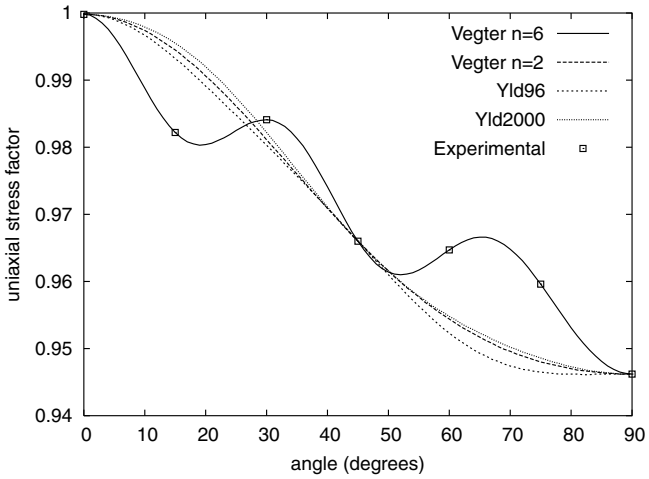


Fig. 6. Predicted and experimental uniaxial stress factors.

experimentally determined for every 15° with respect to the rolling direction. For an interpolation with $n = 6$, all measured values are on the curve, even for the wildly varying uniaxial stress factor. The other yield functions are added for comparison. For an interpolation with $n = 2$ and for the Yld96 and Yld2000 model, the material parameters are based on the 0°, 45° and 90° directions only and are therefore only exact at these points.

If plane strain or shear data are completely lacking, the missing data may be supplemented by data derived from other reliable yield functions, e.g., Yld96 for FCC

metals. If all stress points and strain ratios are obtained in this way, the proposed yield function is just a generic implementation to approximate other yield functions. Recently, Pöhlandt et al. (2002) proposed a Bézier interpolation between only uniaxial and biaxial points. If the plane strain and pure shear points are taken from this simplified yield locus, the currently proposed yield function coincides with theirs.

## 3. Yield function

Virtually all algorithms for the simulation of plastic deformation are based on the notion of a yield function. In order to use existing algorithms, the interpolated yield locus is now cast into a yield function $\phi$, such that $\phi < 0$ in the elastic regime, $\phi = 0$ on the yield locus and $\phi > 0$ in the infeasible stress space outside the yield locus.

### 3.1. Equivalent stress

A yield function in the classical sense is constructed by defining an equivalent stress $\sigma_{\mathrm{eq}}$, that can be determined for any plane stress state by the relation

$$\vec{\sigma} = \sigma_{\mathrm{eq}}\vec{f} = \sigma_{\mathrm{eq}}\left[\vec{A} + 2\mu\left(\vec{B} - \vec{A}\right) + \mu^2\left(\vec{A} + \vec{C} - 2\vec{B}\right)\right], \quad 0 \leqslant \mu \leqslant 1. \tag{11}$$

For a particular stress $\boldsymbol{\sigma}$, the principal stresses $\sigma_1$ and $\sigma_2$ and the orientation $\theta$ are calculated. It is then straightforward to determine the active region in the normalised yield locus – between equi-biaxial and plane strain, between plane strain and uniaxial or between uniaxial and pure shear – and by solution of a quadratic equation the value of $\mu$ can be determined efficiently. The equivalent stress follows easily as $\sigma_1/f_1$ or with the same result as $\sigma_2/f_2$. A yield function $\phi$ that is defined as

$$\phi(\boldsymbol{\sigma}, \varepsilon_{\mathrm{eq}}) = \sigma_{\mathrm{eq}}(\boldsymbol{\sigma}) - \sigma_{\mathrm{f}}(\varepsilon_{\mathrm{eq}}) \tag{12}$$

fulfils the imposed conditions. The direction of the plastic strain rate can be calculated from the derivative of $\phi$ to the stress $\boldsymbol{\sigma}$. Since $\phi$ is continuously differentiable, the plastic strain rate direction is continuous.

### 3.2. Strain rate directions

Based on Drucker's normality principle, the direction of plastic strain rate can be derived from the yield function by

$$\mathrm{d}\boldsymbol{\varepsilon}^{\mathrm{p}} = \mathrm{d}\lambda\frac{\partial\phi}{\partial\boldsymbol{\sigma}}, \tag{13}$$

where $\boldsymbol{\sigma} = \{\sigma_{xx}, \sigma_{yy}, \sigma_{xy}\}$ and $\boldsymbol{\varepsilon} = \{\varepsilon_{xx}, \varepsilon_{yy}, \gamma_{xy}\}$, applying vector notation for the stress and strain tensor. It is convenient to define the stress in the material with respect to the orthotropic axes, therefore the rolling direction is defined to be the $x$-axis and the

transverse direction to be the $y$-axis. The Vegter yield function is defined in the plane stress space as a function of $\mathbf{X} = \{\sigma_1, \sigma_2, \cos 2\theta\}$ and the relation between $\mathbf{X}$ and $\boldsymbol{\sigma}$ is described by:

$$\sigma_1 = \frac{1}{2}\left(\sigma_{xx} + \sigma_{yy} + \sqrt{\left(\sigma_{xx} - \sigma_{yy}\right)^2 + 4\sigma_{xy}^2}\right), \tag{14}$$

$$\sigma_2 = \frac{1}{2}\left(\sigma_{xx} + \sigma_{yy} - \sqrt{\left(\sigma_{xx} - \sigma_{yy}\right)^2 + 4\sigma_{xy}^2}\right), \tag{15}$$

$$\cos 2\theta = \frac{\sigma_{xx} - \sigma_{yy}}{\sqrt{\left(\sigma_{xx} - \sigma_{yy}\right)^2 + 4\sigma_{xy}^2}} = \frac{\sigma_{xx} - \sigma_{yy}}{\sigma_1 - \sigma_2}, \tag{16}$$

$$\sin 2\theta = \frac{2\sigma_{xy}}{\sqrt{\left(\sigma_{xx} - \sigma_{yy}\right)^2 + 4\sigma_{xy}^2}} = \frac{2\sigma_{xy}}{\sigma_1 - \sigma_2}. \tag{17}$$

For the transformation from principal to material axes, the transformation matrix is needed that follows easily from differentiation of (14)–(16) and substitution of (16) and (17):

$$\frac{\partial \mathbf{X}}{\partial \boldsymbol{\sigma}} = \begin{bmatrix} \frac{\partial \sigma_1}{\partial \sigma_{xx}} & \frac{\partial \sigma_1}{\partial \sigma_{yy}} & \frac{\partial \sigma_1}{\partial \sigma_{xy}} \\ \frac{\partial \sigma_2}{\partial \sigma_{xx}} & \frac{\partial \sigma_2}{\partial \sigma_{yy}} & \frac{\partial \sigma_2}{\partial \sigma_{xy}} \\ \frac{\partial \cos 2\theta}{\partial \sigma_{xx}} & \frac{\partial \cos 2\theta}{\partial \sigma_{yy}} & \frac{\partial \cos 2\theta}{\partial \sigma_{xy}} \end{bmatrix} = \begin{bmatrix} \frac{1}{2}(1+\cos 2\theta) & \frac{1}{2}(1-\cos 2\theta) & \sin 2\theta \\ \frac{1}{2}(1-\cos 2\theta) & \frac{1}{2}(1+\cos 2\theta) & -\sin 2\theta \\ \frac{\sin^2 2\theta}{\sigma_1 - \sigma_2} & -\frac{\sin^2 2\theta}{\sigma_1 - \sigma_2} & -\frac{2\sin 2\theta \cos 2\theta}{\sigma_1 - \sigma_2} \end{bmatrix}. \tag{18}$$

With $\phi$ an explicit function of $\mathbf{X}$, the strain rate direction follows from:

$$\frac{\partial \phi}{\partial \boldsymbol{\sigma}} = \left(\frac{\partial \mathbf{X}}{\partial \boldsymbol{\sigma}}\right)^{\mathrm{T}} \frac{\partial \phi}{\partial \mathbf{X}}, \tag{19}$$

where $\partial\phi/\partial\boldsymbol{\sigma}$ and $\partial\phi/\partial\mathbf{X}$ are written as column vectors. With (18) this can be written as

$$\begin{Bmatrix} \frac{\partial \phi}{\partial \sigma_{xx}} \\ \frac{\partial \phi}{\partial \sigma_{yy}} \\ \frac{\partial \phi}{\partial \sigma_{xy}} \end{Bmatrix} = \begin{bmatrix} \frac{1}{2}(1+\cos 2\theta) & \frac{1}{2}(1-\cos 2\theta) & \frac{\sin^2 2\theta}{\sigma_1 - \sigma_2} \\ \frac{1}{2}(1-\cos 2\theta) & \frac{1}{2}(1+\cos 2\theta) & -\frac{\sin^2 2\theta}{\sigma_1 - \sigma_2} \\ \sin 2\theta & -\sin 2\theta & -\frac{2\sin 2\theta \cos 2\theta}{\sigma_1 - \sigma_2} \end{bmatrix} \begin{Bmatrix} \frac{\partial \phi}{\partial \sigma_1} \\ \frac{\partial \phi}{\partial \sigma_2} \\ \frac{\partial \phi}{\partial \cos 2\theta} \end{Bmatrix}. \tag{20}$$

The derivatives of $\phi$ with respect to $\sigma_1$, $\sigma_2$ and $\cos 2\theta$ are elaborated in Appendix B and can be written as:

$$\begin{Bmatrix} \frac{\partial \phi}{\partial \sigma_1} \\ \frac{\partial \phi}{\partial \sigma_2} \\ \frac{\partial \phi}{\partial \cos 2\theta} \end{Bmatrix} = \frac{1}{f_1 \frac{\partial f_2}{\partial \mu} - f_2 \frac{\partial f_1}{\partial \mu}} \begin{Bmatrix} \frac{\partial f_2}{\partial \mu} \\ -\frac{\partial f_1}{\partial \mu} \\ \sigma_{\mathrm{eq}}\left(\frac{\partial f_2}{\partial c}\frac{\partial f_1}{\partial \mu} - \frac{\partial f_1}{\partial c}\frac{\partial f_2}{\partial \mu}\right) \end{Bmatrix}, \tag{21}$$

where $\partial f_1/\partial c$ is the partial derivative of $f_1$ to $\cos 2\theta$ at constant $\mu$. The common multiplier can be regarded as the reciprocal value of the magnitude of the outer product

of $\vec{f}$ and $\partial\vec{f}/\partial\mu$. The outer product will never be zero for a convex yield locus, unless one of both vectors is of size zero. The derivatives of $\vec{f}$ to $\mu$ and cos $2\theta$ are easily obtained from Eq. (2):

$$\frac{\partial\vec{f}}{\partial\mu} = 2\left(\vec{B}-\vec{A}\right) + 2\mu\left(\vec{A}+\vec{C}-2\vec{B}\right), \tag{22}$$

$$\frac{\partial\vec{f}}{\partial c} = \frac{\mathrm{d}\vec{A}}{\mathrm{d}c} + 2\mu\left(\frac{\mathrm{d}\vec{B}}{\mathrm{d}c} - \frac{\mathrm{d}\vec{A}}{\mathrm{d}c}\right) + \mu^2\left(\frac{\mathrm{d}\vec{A}}{\mathrm{d}c} + \frac{\mathrm{d}\vec{C}}{\mathrm{d}c} - 2\frac{\mathrm{d}\vec{B}}{\mathrm{d}c}\right). \tag{23}$$

The derivatives $\mathrm{d}\vec{A}/\mathrm{d}c$ and $\mathrm{d}\vec{C}/\mathrm{d}c$ are readily derived from the Fourier series (5). The derivative of the hinge point $\vec{B}$ depends on the reference points and the strain ratios and is elaborated in Appendix A.

In the equi-biaxial point ($\sigma_1 = \sigma_2$), the direction of the principal stresses is indeterminate and this leads to a singularity that is apparent from the third row in the transformation matrix (18). This singularity can easily be avoided by elaboration of the yield function in case one of the reference points is the equi-biaxial point, as demonstrated in Appendix C.

### 3.3. Equivalent strain

The equivalent plastic strain is, in this work, based on the plastic work principle: the equivalent stress multiplied by the equivalent plastic strain rate should give the same dissipation as the tensorial multiplication of stress tensor and plastic strain rate tensor. This leads to an equivalent plastic strain rate of

$$\dot{\varepsilon}_{\mathrm{eq}} = \frac{\boldsymbol{\sigma} : \dot{\boldsymbol{\varepsilon}}^{\mathrm{p}}}{\sigma_{\mathrm{eq}}}. \tag{24}$$

This equation is independent of the reference frame and can, using (11), conveniently be written with respect to the principal stress directions as

$$\dot{\varepsilon}_{\mathrm{eq}} = \frac{\sigma_1\dot{\varepsilon}^{\mathrm{p}}_{\sigma 1} + \sigma_2\dot{\varepsilon}^{\mathrm{p}}_{\sigma_2}}{\sigma_{\mathrm{eq}}} = f_1\dot{\varepsilon}^{\mathrm{p}}_{\sigma_1} + f_2\dot{\varepsilon}^{\mathrm{p}}_{\sigma_2}. \tag{25}$$

Here, $f_1$ and $f_2$ are completely determined by the current stress state and therefore there is a linear relation between $\dot{\varepsilon}_{\mathrm{eq}}$ and $\dot{\boldsymbol{\varepsilon}}^{\mathrm{p}}$. The equivalent strain is commonly used to define the evolution of isotropic and kinematic work hardening.

## 4. Application

To demonstrate the applicability of the interpolated yield function the reference stresses and normals were determined for an IF-steel and an AlMgSi alloy. Subsequently, the forming limit diagrams for these materials were predicted with several yield criteria and compared with experimentally obtained FLDs. It is well known

that the prediction of an FLD is very sensitive to the applied yield locus and therefore constitutes a serious test for the accuracy of a yield function.

### 4.1. Material parameters

The characteristic stress factors for both materials were obtained from uniaxial tensile tests and plane strain tensile tests in the 0°, 45° and 90° directions and a compression test perpendicular to the sheet plane; they are presented in Table 2. The shear point was based on the measured texture and a subsequent polycrystal analysis. This point, however, is not relevant in the following FLD determination because the minor stress is always kept positive.

All measured points can directly be used as parameters for the interpolated yield locus model. Some freedom still exists for the plane strain point; the second stress component was not measured and can be chosen arbitrarily between the neighbouring two hinge points. A position in the middle between the hinge points results in a relatively high curvature in the equi-biaxial range. Moving the plane strain point upwards, towards the equi-biaxial point, gives a lower curvature. For the AlMgSi alloy, two variations are used, one with the plane strain point in the middle between the neighbouring hinge points and one where the plane strain point is at 10% from the equi-biaxial hinge point. The last one is indicated as 'Vegter flat' in Fig. 8(b). In order to keep the yield function convex, the plane strain points were slightly adapted. The influence of the position of the plane strain point on the FLD is discussed in the next section.

Three other yield functions are considered for comparison: Hill '48, Hill '90 and Yld2000. These yield functions have fewer parameters than measured quantities. The parameters for the Hill '48 function were determined using the 3 $R$-values and the uniaxial yield stress at 0°. For Hill '90, the equi-biaxial stress was used additionally. For the Yld2000 function all $R$-values and uniaxial yield stresses and the equi-biaxial yield stress and strain ratio were used. The exponent $m$ in Yld2000 was set to 6 for IF-steel and 8 for AlMgSi alloy. Alternatively, for Hill '90 and Yld2000, all available experimental data was used in a least-squares fitting process. In this case, the exponent $m$ for the Yld2000 model was also used as a variable. In Figs. 7–10 these models are denoted by "Hill '90 opt" and "Yld2000 opt", respectively.

Table 2
Yield locus parameters for the investigated IF-steel and AlMgSi alloy

| | $\theta$ | $f_{un}$ | $f_{sh}$ | $f_{ps}$ | $f_{bi}$ | $R$ | $\rho_{bi}$ |
|---|---|---|---|---|---|---|---|
| IF | 0° | 1.004 | 0.537 | 1.247 | 1.157 | 1.85 | 0.777 |
| IF | 45° | 0.998 | 0.545 | 1.252 | | 2.06 | |
| IF | 90° | 0.997 | 0.537 | 1.250 | | 2.51 | |
| Al | 0° | 1.021 | 0.560 | 1.061 | 1.004 | 0.64 | 0.889 |
| Al | 45° | 0.987 | 0.640 | 1.037 | | 0.48 | |
| Al | 90° | 1.009 | 0.560 | 1.048 | | 0.76 | |

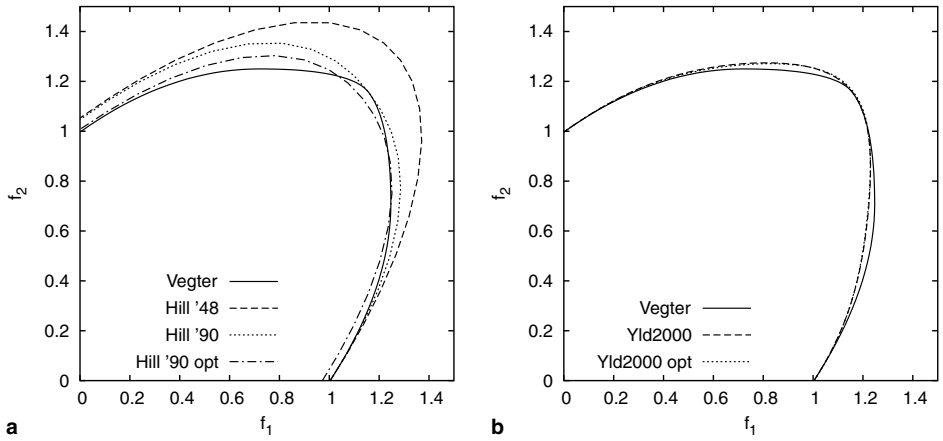


Fig. 7. Yield locus prediction for IF-steel according to different models ($\theta = 0°$).

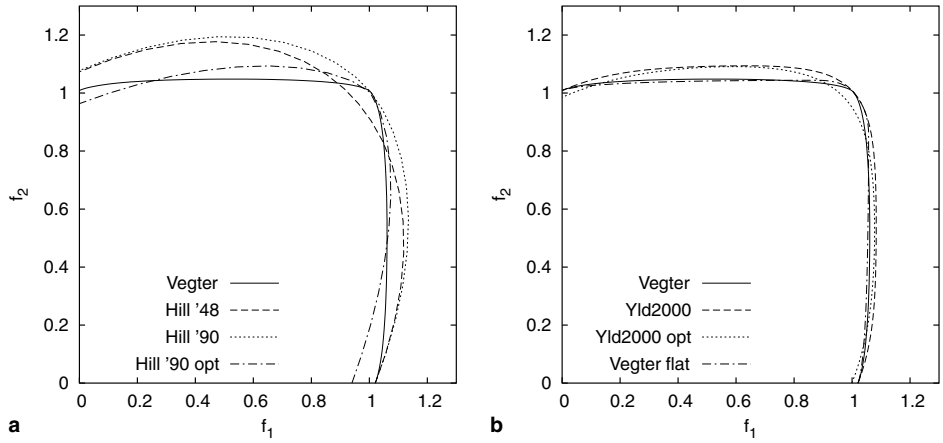


Fig. 8. Yield locus prediction for AlMgSi alloy according to different models ($\theta = 0°$).

Considering that the yield loci for the new yield function are based on measured uniaxial, plane strain and biaxial data, it can be concluded from Figs. 7(a) and 8(a) that the Hill '48 and Hill '90 yield functions give bad predictions for the plane strain stress when the parameters are determined in the standard way. If the parameters for Hill '90 are optimised, the prediction of the plane strain stress improves, but at the cost of a correct uniaxial and equi-biaxial stress.

For the two materials used here, the difference between Yld96 (not shown) and Yld2000 was small. The Yld2000 function directly uses the uniaxial and equi-biaxial stresses and strain ratios and therefore give exact correspondence with the curve for the Vegter function. Figs. 7(b) and 8(b) show that Yld2000 does not predict the experimentally observed plane strain stress, especially for the AlMgSi alloy. This

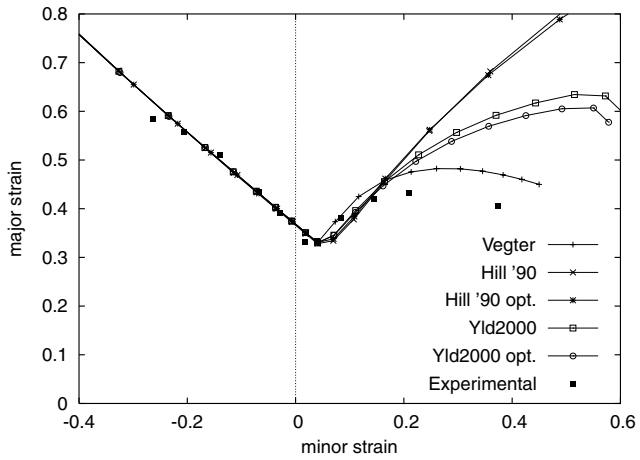


Fig. 9. FLD predictions for the IF-steel (90° to RD) using different yield criteria and comparison with experiments.

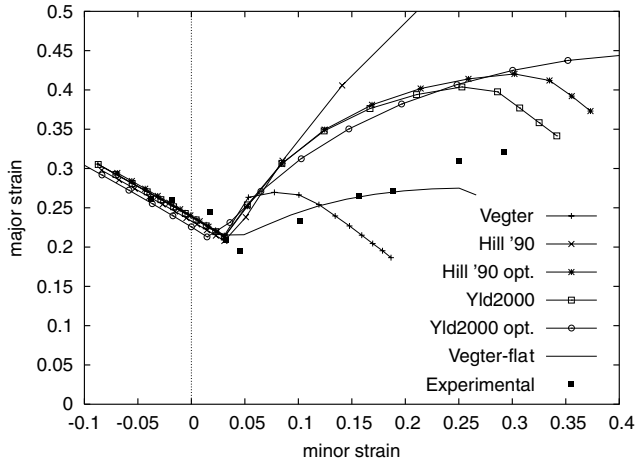


Fig. 10. FLD predictions for the AlMgSi alloy (90° to RD) using different yield criteria and comparison with experiments.

is hardly improved by using optimised parameters because of the large misfit of the pure shear stress at 45°.

Apart from the yield function, a predicted FLD is sensitive to the hardening function. Here, isotropic hardening is assumed with an extended Bergström relation (Bergström, 1969; Van Liempt, 1994) to which the effect of strain rate and temperature were added as described by Krabiell and Dahl (1981). The flow stress is given by

$$\sigma_f = \sigma_0 + \Delta\sigma_m\left[\beta(\varepsilon_{eq}+\varepsilon_0) + \left(1 - e^{-\Omega(\varepsilon_{eq}+\varepsilon_0)}\right)^{n'}\right] + \sigma_0^*\left[1 + \frac{kT}{\Delta G_0}\ln\left(\frac{\dot{\varepsilon}_{eq}}{\dot{\varepsilon}_0}\right)\right]^{m'}. \quad (26)$$

This hardening relation proved to be sufficiently accurate (Vegter, 1991). The hardening parameters for both materials are presented in Table 3.

### 4.2. Forming limit diagrams

FLD experiments were carried out by stretching Nakazima strips over a hemispherical punch with a diameter of 75 mm. A special rubber like foil was used as a lubricant on the punch head. The instability strains were derived in failed specimens.

Numerically, FLDs were determined for both materials based on the Marciniak–Kuczinsky (M–K) analysis (Marciniak and Kuczynski, 1967), using an initial thickness defect of 0.01%. For the left-hand side (LHS) of the FLD the original M–K approach has been adapted; the strain state outside the groove was assumed to be proportional to the one inside the groove. For the simulations a two stage deformation process has been chosen. Due to the dome shape of the punch, all specimens were assumed to be bi-axially pre-strained up to a level of 0.05 ($\varepsilon_1 = \varepsilon_2 = 0.05$). From there different strain combinations will occur depending on the width of the specimens. Due to the assumption of proportional hardening, the LHS of the FLD is determined only by the strain hardening and strain rate relation and does not depend on the shape of the yield criterion. Therefore, the initial thickness defect of 0.01% and the amount of biaxial pre-strain were adjusted for both materials to the LHS of the experimental FLDs. The assumption of an initial thickness defect remains a weak point of the M–K analysis.

The different yield loci led to significantly different results in the prediction of the right-hand side (RHS) of the FLD (Figs. 9 and 10). Due to the prediction of a too large plane strain major stress with the Hill '90 criterion, the FLD is largely over-estimated on the RHS for both materials. The optimised parameters improved the predicted FLD for the AlMgSi alloy, but not for the IF-steel.

With the Yld2000 criterion the predicted FLDs improved a lot compared to Hill '90, but the maximum strain in biaxial tension is still over-estimated for both materials. Using optimised parameters for the yield locus improved the predicted FLD for IF-steel, but the prediction for AlMgSi alloy deteriorated. With the Vegter criterion, the M–K analysis gives a much better prediction of the FLD for

Table 3
Hardening parameters for the investigated IF-steel and AlMgSi alloy

| | $\sigma_0$ (MPa) | $\Delta\sigma_m$ (MPa) | $\beta$ | $\Omega$ | $\varepsilon_0$ | $n'$ | $\sigma_0^*$ (MPa) | $\Delta G_0$ (eV) | $m'$ | $\dot{\varepsilon}_0$ ($s^{-1}$) |
|---|---|---|---|---|---|---|---|---|---|---|
| IF | 96.2 | 271.0 | 0.25 | 9.27 | 0.005 | 0.75 | 600.0 | 0.8 | 2.2 | $10^8$ |
| Al | 107.1 | 179.6 | 0.25 | 8.07 | 0.000 | 0.75 | 20.0 | 0.8 | 1.0 | $10^8$ |

IF-steel. For the AlMgSi alloy, however, the Vegter criterion under-estimates the FLD in the equi-biaxial range. This is attributed to a too high curvature of the yield locus near the equi-biaxial point. The curvature can be reduced by shifting the plane strain minor stress towards the equi-biaxial point in the Vegter criterion, indicated as Vegter flat in Fig. 8(b). Although this change can hardly be seen in the yield locus, the correspondence with the measured FLD is improved significantly. This effect shows the extreme sensitivity of the FLD prediction for the shape of the yield locus and demonstrates the necessity for an accurate yield locus description.

## 5. Conclusions

A new plane stress yield function was introduced that is based on 4 different stress states for an arbitrary number of directions with respect to the main material axis, commonly the rolling direction. The yield function is based on a yield locus description that applies second order Bézier interpolations. If 3 directions are used, the new yield function requires 17 independent parameters, that can readily be derived from equi-biaxial, plane strain, uniaxial and shear tests in the 3 directions or from a polycrystal analysis. Although the number of parameters is large, the transformation of experimental or theoretical data to the model parameters is straightforward and does not lead to nonlinear sets of equations.

Each Bézier interpolation is used only in a limited part of the yield locus, therefore the new criterion is very flexible and can adapt to many materials. Application to a BCC and an FCC material was demonstrated. By using more than 3 directions also materials that develop 6 or 8 ears in cylindrical deep drawing can be modelled. Because of the piecewise quadratic interpolations, the evaluation of the yield function is very efficient. In an initial FEM implementation, CPU times were comparable with that for the quadratic Hill model.

The prediction of forming limits once again showed a large influence of the shape of the yield function between the plane strain and equi-biaxial stress states. Using experimentally determined plane strain values significantly improved the predicted FLDs, compared to yield functions that are only based on uniaxial and equi-biaxial data. By adapting the minor stress of the plane strain point, the new criterion could successfully be fitted to an experimental FLD. This observation presents an alternative way to determine the minor stress in a plane strain state, that could otherwise only be obtained by a biaxial test, using a cruciform specimen.

## Acknowledgements

The authors specially thank Hermen Pijlman for his work to make this model suitable for implementation in FE-codes. The development of material tests by Yuguo An, Hermen Pijlman, Joop Brinkman and Jan Heijne made it possible to determine the parameters for the materials investigated.

## Appendix A. Hinge point calculation

Given 2 reference points $\vec{A}$ and $\vec{C}$ and the normals to the yield locus in these points $\vec{n}$ and $\vec{m}$, the hinge point $\vec{B}$ can be calculated from the set of equations:

$$\begin{aligned}(\vec{B}-\vec{A})\cdot\vec{n}&=0,\\(\vec{B}-\vec{C})\cdot\vec{m}&=0,\end{aligned}\tag{A.1}$$

which results in:

$$B_1=\frac{m_2(n_1A_1+n_2A_2)-n_2(m_1C_1+m_2C_2)}{n_1m_2-m_1n_2},\tag{A.2}$$

$$B_2=\frac{n_1(m_1C_1+m_2C_2)-m_1(n_1A_1+n_2A_2)}{n_1m_2-m_1n_2}.\tag{A.3}$$

The derivative of the hinge point with respect to $\cos 2\theta$ is determined from

$$\frac{\mathrm{d}}{\mathrm{d}c}\begin{bmatrix}n_1 & n_2\\ m_1 & m_2\end{bmatrix}\begin{Bmatrix}B_1\\B_2\end{Bmatrix}+\begin{bmatrix}n_1 & n_2\\ m_1 & m_2\end{bmatrix}\frac{\mathrm{d}}{\mathrm{d}c}\begin{Bmatrix}B_1\\B_2\end{Bmatrix}=\frac{\mathrm{d}}{\mathrm{d}c}\begin{Bmatrix}n_1A_1+n_2A_2\\m_1C_1+m_2C_2\end{Bmatrix},\tag{A.4}$$

such that

$$\begin{bmatrix}n_1 & n_2\\ m_1 & m_2\end{bmatrix}\begin{Bmatrix}\frac{\mathrm{d}B_1}{\mathrm{d}c}\\\frac{\mathrm{d}B_2}{\mathrm{d}c}\end{Bmatrix}=\begin{Bmatrix}P_1\\P_2\end{Bmatrix},\tag{A.5}$$

with

$$\begin{Bmatrix}P_1\\P_2\end{Bmatrix}=\begin{Bmatrix}n_1\frac{\mathrm{d}A_1}{\mathrm{d}c}+\frac{\mathrm{d}n_1}{\mathrm{d}c}(A_1-B_1)+n_2\frac{\mathrm{d}A_2}{\mathrm{d}c}+\frac{\mathrm{d}n_2}{\mathrm{d}c}(A_2-B_2)\\m_1\frac{\mathrm{d}C_1}{\mathrm{d}c}+\frac{\mathrm{d}m_1}{\mathrm{d}c}(C_1-B_1)+m_2\frac{\mathrm{d}C_2}{\mathrm{d}c}+\frac{\mathrm{d}m_2}{\mathrm{d}c}(C_2-B_2)\end{Bmatrix},\tag{A.6}$$

hence

$$\begin{Bmatrix}\frac{\mathrm{d}B_1}{\mathrm{d}c}\\\frac{\mathrm{d}B_2}{\mathrm{d}c}\end{Bmatrix}=\frac{1}{n_1m_2-m_1n_2}\begin{Bmatrix}P_1m_2-P_2n_2\\P_2n_1-P_1m_1\end{Bmatrix}.\tag{A.7}$$

If the (non-unit) normal vectors are constructed from the strain ratios, the derivatives of normal vectors follow from

$$\vec{n}=\begin{Bmatrix}n_1\\n_2\end{Bmatrix}=\begin{Bmatrix}1\\\rho\end{Bmatrix}\Rightarrow\frac{\mathrm{d}\vec{n}}{\mathrm{d}c}=\begin{Bmatrix}\frac{\mathrm{d}n_1}{\mathrm{d}c}\\\frac{\mathrm{d}n_2}{\mathrm{d}c}\end{Bmatrix}=\begin{Bmatrix}0\\\frac{\mathrm{d}\rho}{\mathrm{d}c}\end{Bmatrix},\tag{A.8}$$

where $\mathrm{d}\rho/\mathrm{d}c$ is easily derived from the Fourier series (5) or, for the equi-biaxial point, from (9)

$$\frac{\mathrm{d}\rho_{\mathrm{bi}}}{\mathrm{d}c}=2\frac{\rho_{\mathrm{bi},0}^2-1}{\left[\rho_{\mathrm{bi},0}+1-(\rho_{\mathrm{bi},0}-1)\cos 2\theta\right]^2}.\tag{A.9}$$

In this work there is no need to normalise the normal vectors.

## Appendix B. Partial derivatives of $\phi$ to $\sigma_1$, $\sigma_2$ and $\cos 2\theta$

In this section the yield function $\phi(\sigma_1, \sigma_2, \cos 2\theta)$ and the interpolation functions $f_1(\mu, c)$ and $f_2(\mu, c)$ are considered. The parameter $c$ is identical to $\cos 2\theta$, but has been given another symbol in order to clearly distinguish the partial derivative with respect to $\cos 2\theta$ at constant $\sigma_1$ and $\sigma_2$ and with respect to $c$ at constant $\mu$

$$\frac{\partial f_i(\mu, c)}{\partial \cos 2\theta} = \frac{\partial f_i}{\partial c}\frac{\partial c}{\partial \cos 2\theta} + \frac{\partial f_i}{\partial \mu}\frac{\partial \mu}{\partial \cos 2\theta} = \frac{\partial f_i}{\partial c} + \frac{\partial f_i}{\partial \mu}\frac{\partial \mu}{\partial \cos 2\theta}, \quad (i = 1, 2). \tag{B.1}$$

From the definition of $c$ one easily obtains

$$\frac{\partial c}{\partial \cos 2\theta} = 1 \quad \text{and} \quad \frac{\partial c}{\partial \sigma_1} = \frac{\partial c}{\partial \sigma_2} = 0. \tag{B.2}$$

The principal stresses are related to $\sigma_{\text{eq}}$, $\mu$ and $c$ by:

$$\begin{aligned} \sigma_1 &= \sigma_{\text{eq}} f_1(\mu, c), \\ \sigma_2 &= \sigma_{\text{eq}} f_2(\mu, c). \end{aligned} \tag{B.3}$$

The derivative of $\phi$ with respect to $\sigma_1$ can be derived implicitly when $\sigma_1$ and $\sigma_2$ are differentiated with respect to $\sigma_1$. With $\sigma_{\text{eq}} = \phi + \sigma_{\text{f}}$ and $\sigma_{\text{f}}$ being independent of $\sigma_1$, $\sigma_2$ and $\cos 2\theta$ we can derive:

$$\begin{aligned} \frac{\partial \sigma_1}{\partial \sigma_1} &= 1 = \frac{\partial f_1(\mu, c)}{\partial \sigma_1}\sigma_{\text{eq}} + \frac{\partial \phi}{\partial \sigma_1} f_1(\mu, c), \\ \frac{\partial \sigma_2}{\partial \sigma_1} &= 0 = \frac{\partial f_2(\mu, c)}{\partial \sigma_1}\sigma_{\text{eq}} + \frac{\partial \phi}{\partial \sigma_1} f_2(\mu, c). \end{aligned} \tag{B.4}$$

Since $\cos 2\theta$ and $\sigma_1$ are independent it follows that:

$$\begin{aligned} \frac{\partial f_1(\mu, c)}{\partial \mu}\frac{\partial \mu}{\partial \sigma_1}\sigma_{\text{eq}} + \frac{\partial \phi}{\partial \sigma_1} f_1(\mu, c) = 1, \\ \frac{\partial f_2(\mu, c)}{\partial \mu}\frac{\partial \mu}{\partial \sigma_1}\sigma_{\text{eq}} + \frac{\partial \phi}{\partial \sigma_1} f_2(\mu, c) = 0. \end{aligned} \tag{B.5}$$

Solving this set of equations for $\partial\phi/\partial\sigma_1$, eliminating $\partial\mu/\partial\sigma_1$, yields

$$\frac{\partial \phi}{\partial \sigma_1} = \frac{\frac{\partial f_2}{\partial \mu}}{f_1 \frac{\partial f_2}{\partial \mu} - f_2 \frac{\partial f_1}{\partial \mu}}. \tag{B.6}$$

A similar procedure for $\sigma_2$ results in

$$\frac{\partial \phi}{\partial \sigma_2} = \frac{-\frac{\partial f_1}{\partial \mu}}{f_1 \frac{\partial f_2}{\partial \mu} - f_2 \frac{\partial f_1}{\partial \mu}}. \tag{B.7}$$

The derivative of $\phi$ with respect to $\cos 2\theta$ can be derived when $\sigma_1$ and $\sigma_2$ are differentiated with respect to $\cos 2\theta$:

$$\begin{aligned}\frac{\partial\sigma_1}{\partial\cos 2\theta} = 0 &= \frac{\partial f_1(\mu,c)}{\partial\cos 2\theta}\sigma_{\mathrm{eq}} + \frac{\partial\phi}{\partial\cos 2\theta}f_1(\mu,c),\\ \frac{\partial\sigma_2}{\partial\cos 2\theta} = 0 &= \frac{\partial f_2(\mu,c)}{\partial\cos 2\theta}\sigma_{\mathrm{eq}} + \frac{\partial\phi}{\partial\cos 2\theta}f_2(\mu,c),\end{aligned} \tag{B.8}$$

or by substitution of (B.1):

$$\begin{aligned}\left(\frac{\partial f_1}{\partial c} + \frac{\partial f_1}{\partial\mu}\frac{\partial\mu}{\partial\cos 2\theta}\right)\sigma_{\mathrm{eq}} + \frac{\partial\phi}{\partial\cos 2\theta}f_1(\mu,c),\\ \left(\frac{\partial f_2}{\partial c} + \frac{\partial f_2}{\partial\mu}\frac{\partial\mu}{\partial\cos 2\theta}\right)\sigma_{\mathrm{eq}} + \frac{\partial\phi}{\partial\cos 2\theta}f_2(\mu,c).\end{aligned} \tag{B.9}$$

Solving this set of equations for $\partial\phi/\partial\cos 2\theta$, eliminating $\partial\mu/\partial\cos 2\theta$, yields:

$$\frac{\partial\phi}{\partial\cos 2\theta} = \sigma_{\mathrm{eq}}\frac{\frac{\partial f_2}{\partial c}\frac{\partial f_1}{\partial\mu} - \frac{\partial f_1}{\partial c}\frac{\partial f_1}{\partial\mu}}{f_1\frac{\partial f_2}{\partial\mu} - f_2\frac{\partial f_1}{\partial\mu}}. \tag{B.10}$$

## Appendix C. The equi-biaxial singularity

At the equi-biaxial point ($\sigma_1 = \sigma_2$) a singularity appears in Eq. (20). This singularity dissolves by elaboration of the matrix–vector multiplication, therefore the third column of the matrix in (20) is multiplied and the corresponding item $\partial\phi/\partial c$ is divided by $\sigma_1 - \sigma_2$.

$$\begin{Bmatrix}\frac{\partial\phi}{\partial\sigma_{xx}}\\ \frac{\partial\phi}{\partial\sigma_{yy}}\\ \frac{\partial\phi}{\partial\sigma_{xy}}\end{Bmatrix} = \frac{1}{f_1\frac{\partial f_2}{\partial\mu} - f_2\frac{\partial f_1}{\partial\mu}}\begin{bmatrix}\frac{1}{2}(1+c) & \frac{1}{2}(1-c) & s^2\\ \frac{1}{2}(1-c) & \frac{1}{2}(1+c) & -s^2\\ s & -s & -2sc\end{bmatrix}\begin{Bmatrix}\frac{\partial f_2}{\partial\mu}\\ -\frac{\partial f_1}{\partial\mu}\\ \frac{\sigma_{\mathrm{eq}}}{\sigma_1-\sigma_2}\left(\frac{\partial f_2}{\partial c}\frac{\partial f_1}{\partial\mu} - \frac{\partial f_1}{\partial c}\frac{\partial f_2}{\partial\mu}\right)\end{Bmatrix}. \tag{C.1}$$

Now, obviously, only the third component of the last vector is singular for $\sigma_1 = \sigma_2$. We can write: $\sigma_i = \sigma_{\mathrm{eq}} f_i(\mu,c)$ where $f_i$ is defined as

$$f_i(\mu,c) = (1-\mu)^2 A_i(c) + 2\mu(1-\mu)B_i(c) + \mu^2 C_i(c) \tag{C.2}$$

and therefore

$$\frac{\partial f_i}{\partial\mu} = 2[-(1-\mu)A_i(c) + (1-2\mu)B_i(c) + \mu C_i(c)] \tag{C.3}$$

and

$$\frac{\partial f_i}{\partial c} = (1-\mu)^2\frac{\partial A_i}{\partial c} + 2\mu(1-\mu)\frac{\partial B_i}{\partial c} + \mu^2\frac{\partial C_i}{\partial c}. \tag{C.4}$$

The difference in principal stresses is

$$\sigma_1 - \sigma_2 = \sigma_{\mathrm{eq}}\Big\{(1-\mu)^2[A_1 - A_2] + 2\mu(1-\mu)[B_1 - B_2] + \mu^2[C_1 - C_2]\Big\}, \tag{C.5}$$

such that

$$\frac{\sigma_1-\sigma_2}{\sigma_{\mathrm{eq}}}=(1-\mu)^2[A_1-A_2]+2\mu(1-\mu)[B_1-B_2]+\mu^2[C_1-C_2]. \tag{C.6}$$

The part between brackets in the third component is written as

$$\begin{aligned}\frac{\partial f_2}{\partial c}\frac{\partial f_1}{\partial \mu}-\frac{\partial f_1}{\partial c}\frac{\partial f_2}{\partial \mu}&=2\left[(1-\mu)^2\frac{\partial A_2}{\partial c}+2\mu(1-\mu)\frac{\partial B_2}{\partial c}+\mu^2\frac{\partial C_2}{\partial c}\right]\frac{\partial f_1}{\partial \mu}\\&\quad-2\left[(1-\mu)^2\frac{\partial A_1}{\partial c}+2\mu(1-\mu)\frac{\partial B_1}{\partial c}+\mu^2\frac{\partial C_1}{\partial c}\right]\frac{\partial f_2}{\partial \mu}.\end{aligned} \tag{C.7}$$

If $A$ represents the equi-biaxial point then $A_1 = A_2 = f_{\mathrm{bi}}$ which is independent of the direction $\theta$ and therefore $\partial A_1/\partial c = \partial A_2/\partial c = 0$. The numerator and denominator can then be divided by $\mu$ and the vector becomes completely regular

$$\sigma_{\mathrm{eq}}\frac{\frac{\partial f_2}{\partial c}\frac{\partial f_1}{\partial \mu}-\frac{\partial f_1}{\partial c}\frac{\partial f_2}{\partial \mu}}{\sigma_1-\sigma_2}=\frac{2\left[2(1-\mu)\frac{\partial B_2}{\partial c}+\mu\frac{\partial C_2}{\partial c}\right]\frac{\partial f_1}{\partial \mu}-\left[2(1-\mu)\frac{\partial B_1}{\partial c}+\mu\frac{\partial C_1}{\partial c}\right]\frac{\partial f_2}{\partial \mu}}{2(1-\mu)(B_1-B_2)+\mu(C_1-C_2)}. \tag{C.8}$$

This expression can be used for the complete Bézier curve between the equi-biaxial and the plane strain point and not only for a limit $\varepsilon \to 0$ around the equi-biaxial point.

## References

An, Y., Vegter, H., 1998. The difference in plastic behaviour between bulging test and through thickness compression test for sheet steels and Al-alloys. In: IDDRG Working Groups Meeting, Genval, Belgium.

Banabic, D., Aretz, H., Comsa, D.S., Paraianu, L., 2005. An improved analytical description of orthotropy in metallic sheets. International Journal of Plasticity 21, 493–512.

Banabic, D., Kuwabara, T., Balan, T., Comsa, D.S., Julean, D., 2003. Nonquadratic yield criterion for orthotropic sheet metals under plane-stress conditions. International Journal of Mechanical Sciences 45, 797–811.

Barlat, F., Aretz, H., Yoon, J.W., Karabin, M.E., Brem, J.C., Dick, R.E., 2005. Linear transformation-based anisotropic yield functions. International Journal of Plasticity 21, 1009–1039.

Barlat, F., Becker, R.C., Hayashida, Y., Maeda, Y., Yanagawa, M., Chung, K., Brem, J.C., Lege, D.J., Matsui, K., Murtha, S.J., Hattori, S., 1997a. Yielding description for solution strengthened aluminium alloys. International Journal of Plasticity 13, 385–401.

Barlat, F., Brem, J.C., Yoon, J.W., Chung, K., Dick, R.E., Lege, D.J., Pourboghrat, F., Choi, S.-H., Chu, E., 2003. Plane stress yield function for aluminum alloy sheets – part 1: theory. International Journal of Plasticity 19, 1297–1319.

Barlat, F., Lege, D.J., Brem, J.C., 1991. A six-component yield function for anisotropic materials. International Journal of Plasticity 7, 693–712.

Barlat, F., Lian, J., 1989. Plastic behavior and stretchability of sheet metals. part I: A yield function for orthotropic sheets under plane stress conditions. International Journal of Plasticity 5, 51–66.

Barlat, F., Maeda, Y., Chung, K., Yanagawa, M., Brem, J.C., Hayashida, Y., Lege, D.J., Matsui, K., Murtha, S.J., Hattori, S., Becker, R.C., Makosey, S., 1997b. Yield function development for aluminium alloy sheets. Journal of the Mechanics and Physics of Solids 45, 1727–1763.

Bergström, Y., 1969. Dislocation model for the stress–strain behaviour of polycrystalline Fe with special emphasis on the variation of the densities of mobile and immobile dislocations. Materials Science and Engineering 5, 193–200.

Bézier, P., 1986. Courbes et Surfaces. Vol. 4 of Séries Mathématiques et CAO, Hermes, Paris.

Bron, F., Besson, J., 2004. A yield function for anisotropic materials – application to aluminum alloys. International Journal of Plasticity 20, 937–963.

Butuc, M.C., Banabic, D., Barata da Rocha, A., Gracio, J.J., Ferreira Duarte, J., Jurco, P., Comsa, D.S., 2002. The performance of Yld96 and BBC2000 yield functions in forming limit predictions. Journal of Materials Processing Technology 125–126, 281–286.

Hill, R., 1948. A theory of the yielding and plastic flow of anisotropic metals. Proceedings of the Royal Society of London 193 (Series A), 281–297.

Hill, R., 1979. Theoretical plasticity of textured aggregates. Mathematical Proceedings of the Cambridge Philosophical Society 85, 179–191.

Hill, R., 1990. Constitutive modelling of orthotropic plasticity in sheet metals. Journal of the Mechanics and Physics of Solids 38, 405–417.

Hill, R., 1993. A user-friendly theory of orthotropic plasticity in sheet metals. International Journal of Mechanical Sciences 35, 19–25.

Hoferlin, E., van Bael, A., van Houtte, P., Steyaert, G., Maré, C.D., 1998. Biaxial tests on cruciform specimens for the validation of crystallographic yield loci. Journal of Materials Processing Technology 80–81, 545–550.

Karafillis, A.P., Boyce, M.C., 1993. A general anisotropic yield criterion using bounds and a transformation weighting tensor. Journal of the Mechanics and Physics of Solids 41, 1859–1886.

Krabiell, A., Dahl, W., 1981. Zum Einfluss von Temperatur und Dehngeschwindigkeit auf die Streckgrenze von Baustählen unterschiedlicher Festigkeit. Archiv für das Eisenhüttenwesen 52, 429–436.

Kuwabara, T., Kuroda, M., Tvergaard, V., Nomura, K., 2000. Use of abrupt strain path change for determining subsequent yield surface: experimental study with metal sheets. Acta Materialia 48, 2071–2079.

Kuwabara, T., van Bael, A., Iizuka, E., 2002. Measurement and analysis of yield locus and work hardening characteristics of steel sheets with different *R*-values. Acta Materialia 50, 3717–3729.

Marciniak, Z., Kuczynski, K., 1967. Limit strains in processing of stretch forming sheet metal. International Journal of Mechanical Sciences 9, 609–620.

Müller, W., Pöhlandt, K., 1996. New experiments for determining yield loci of sheet material. Journal of Materials Processing Technology 60, 643–648.

Pijlman, H.H., 2001. Sheet material characterisation by multi-axial experiments. Ph.D. Thesis, University of Twente.

Pijlman, H.H., Huétink, J., Carleer, B.D., Vegter, H., 1998. Application of the Vegter yield criterion and a physically based hardening rule on simulation of sheet forming. In: Huétink, J., Baaijens, F.P.T. (Eds.), Simulation of Materials Processing: Theory, Methods and Applications. Balkema, Rotterdam, pp. 763–768.

Pöhlandt, K., Banabic, D., Lange, K., 2002. Equi-biaxial anisotropy coefficient used to describe the plastic behavior of sheet metal. In: Pietrzyk, M., Mitura, Z., Kaczmar, J. (Eds.), The 5th International ESAFORM Conference on Material Forming, pp. 723–726.

Tong, W., Tao, H., Jiang, X., 2004. Modeling the rotation of orthotropic axes of sheet metals subjected to off-axis uniaxial tension. Journal of Applied Mechanics 71, 521–531.

Tozawa, N., 1978. Plastic deformation behavior under the conditions of combined stress. In: Koistinen, D.P., Wang, N.-M. (Eds.), Mechanics of Sheet Metal Forming. Plenum Press, New York, pp. 81–110.

Van Liempt, P., 1994. Workhardening and substructural geometry of metals. Journal of Materials Processing Technology 45, 459–464.

Vegter, H., 1991. On the plastic behaviour of steel during sheet forming. Ph.D. Thesis, University of Twente.

Vegter, H., An, Y., Pijlman, H.H., Huétink, J., 1999a. Advanced mechanical testing on aluminium alloys and low carbon steels for sheet forming. In: Gelin, J.C., Picart, P. (Eds.), Proceedings NUMI-SHEET'99, Besançon, pp. 3–8.

Vegter, H., An, Y., Pijlman, H.H., Huétink, J., 1999b. Different approaches to describe the plastic material behaviour of steel and aluminium-alloys in sheet forming. In: Covas, J.A. (Ed.), Proceedings of the 2nd ESAFORM Conference on Material Forming. Guimarães, pp. 127–132.

Vegter, H., Drent, P., Huétink, J., 1995. A planar isotropic yield criterion based on mechanical testing at multi-axial stress states. In: Shen, S.-F., Dawson, P.R. (Eds.), Simulation of Materials Processing: Theory, Methods and Applications. Balkema, Rotterdam, pp. 345–350.

Vegter, H., ten Horn, C.H.L.J., An, Y., Atzema, E.H., Pijlman, H.H., van den Boogaard, A.H., Huétink, J., 2003. Characterisation and modelling of the plastic material behaviour and its application in sheet metal forming simulation. In: Oñate, E., Owen, D.R.J. (Eds.), 7th International Conference on Computational Plasticity, Barcelona (on CD-ROM).

Woodthorpe, J., Pearce, R., 1970. The anomalous behaviour of aluminium sheet under balanced biaxial tension. International Journal of Mechanical Sciences 12, 341–346.

Wu, P.D, Jain, M., Savoie, J., MacEwen, S.R., Tuğcu, P., Neale, K.W., 2003. Evaluation of anisotropic yield functions for aluminum sheets. International Journal of Plasticity 19, 121–138.